Postprint of: Szydłowski C., Smakosz Ł., Stienss M., Górski J., The use of a two-phase Monte Carlo material model to reflect the dispersion of asphalt concrete fracture parameters, THEORETICAL AND APPLIED FRACTURE MECHANICS, Vol. 119 (2022), 103326, DOI: 10.1016/j.tafmec.2022.103326

The use of a two-phase Monte Carlo material model to reflect the dispersion of asphalt concrete fracture parameters

Cezary Szydłowski [a)], Łukasz Smakosz [b)], Marcin Stienss [c)] and Jarosław Górski [d)]

Faculty of Civil and Environmental Engineering, Gdansk University of Technology
Narutowicza 11/12, 80-233 Gdansk, Poland

[a)] Corresponding author: cezszydl@pg.edu.pl
[b)] luksmako@pg.edu.pl
[c)] mstienss@pg.edu.pl
[d)] jgorski@pg.edu.pl

Abstract

The work covers comprehensive laboratory tests of semi-circular bending (SCB) of asphalt concrete samples. The results of two test series, including four and 32 SCB specimens, indicate a substantial scatter of force-deflection (*F*-*d*) histories. The numerical analysis is aimed to reflect the maximum breaking load and fracture energy of the samples, pointing out their random character. The original simulation-based fictitious Monte Carlo material model was introduced. The authors' algorithm randomly assigns asphalt mortar and coarse aggregate parameters to the finite elements of the numerical model. As a result, sets of random fields are generated to reflect the two-phase material distribution in the samples. The model parameters are numerically adjusted based on laboratory test results of the initial four SCB specimens. In the course of model verification, the 32-sample computations were compared with the laboratory data. The results of FEM simulations are consistent with laboratory test results, including dispersion of fracture parameters. The proposed computational algorithm with a two-phase material model is ready to be implemented in the analysis of actual road pavement constructions and may support the design process.

Keywords

asphalt concrete; laboratory tests; SCB specimens; numerical simulation; probabilistic analysis; Monte Carlo material model

1. Introduction

The fracture process of mineral-asphalt mixtures raises road operation costs and reduces the comfort and safety of road explorers. This field is illustrated by comprehensive literature references concerning laboratory testing. The tested specimens of various shapes and dimensions exhibit significant scatter of a multitude of parameters: the maximum force and relative displacement, initial specimen stiffness and softening, fracture energy and toughness, and others. Thus the laboratory test descriptions are primarily statistical in their nature [1]. For example, reliability estimation of various types of composite specimens was addressed in [2]. The work [3] proves that the wheel tracking test results show significant scatter. Regression analysis becomes a standard tool to assess fracture energy of mineral-asphalt mixtures [4]. The impact of size effect and support conditions on the results is essential in laboratory testing [5,6]. Probabilistic material models and element reliability estimation are considered at the design stage [7,8]. New solutions and technologies, e.g., balance mix design [9], are investigated to improve the quality of mixtures with emphasis on their fracture toughness.

The scatter of laboratory results is reflected in numerical simulations mapping the specimen fracture course. Due to the heterogeneity of the material, including bituminous binders, mineral aggregate, and voids, it is hard to build effective numerical models. Constitutive relations are controlled by a number of factors: temperature dependency, aggregate layout, crack onset and propagation, contact between aggregate and bituminous material, cyclic load action, moisture damage, scale effect, and more; universal material relations are in fact out of reach. Actual computational models usually denote a limited application domain. The features of mineral-asphalt mixtures make it possible to perform multi-level modeling, i.e., macroscale, mesoscale and multiscale. Precise mapping of mixture structure is possible using image correlation [10,11] and X-ray Computed Tomography [6,12,13]. The impact of specimen FE discretization is addressed in [14]. The models consider the random character of asphalt mixture, making the material structure homogenized both in two-dimensional and three-dimensional patterns, see [15–17]. Estimating model parameters involves a representative volume element (RVE) [15,18]. This approach is included in works dedicated to soils [19] or concrete [20]. Research [21,22] incorporates random variables as well as isotropic and anisotropic random fields to reflect the variability of mineral-asphalt mixtures. A similar approach is presented in [23]; here, the combination of Karhunen-Loeve (KL) expansion and probabilistic collocation method (PCM) is employed to cover rock failure

uncertainty. Another analytical technique is discrete element approach (DEM) [24]. Material fracture is usually simulated by standard cohesive elements located in the specimen damage zone [25–27] or the entire analyzed domain [28,29]. Cohesive links are frequent in numerical models, allowing for precise fracture course mapping in aggregate and bitumen mortar connections. However, such an approach brings a challenge to specimen modeling; moreover, the database lacks many model parameters of aggregate, bitumen mortar, and their interface.

Laboratory test results of composite materials, such as asphalt concrete, are usually scattered. Thus, performing high-precision specimen structure mapping and exact simulation of the specimen damage process in such a heterogeneous medium seems to have limited practical applications. Engineering algorithms are intended to cover global damage, including result scatter assessment, standard deviation, median estimation, etc. Thus, the proposed algorithm brings a compromise. The original simplified model does not reflect the actual material; instead, it is a quasi-continuum model for the global performance of mineral-asphalt mixture elements. The proposed model randomly prescribes aggregate and bitumen mortar parameters to finite elements. Hence several algorithms are proposed to form a random material structure, from a crude sampling of individual elements to advanced random field applications. It can be described as a Monte Carlo simulation-based constitutive model. Here, standard ABAQUS procedures are applied [30]; simulation of uncertain material parameters employs the authors' code only. Since simulation concerns the damage process of a notched specimen, i.e., a strict crack propagation zone, cohesive elements are assumed along the symmetry axis.

The numerical analysis follows the laboratory tests of semi-circular bending (SCB) of specimens with 10 mm notch depth. SCB specimens were chosen for testing due to simple fabrication and application in many previous research works. Two test groups were prepared, one with four specimens (normative number of samples) and the second with 32 specimens (expanded testing). Results from the second group of samples were used to perform a comprehensive statistical scatter assessment of fracture parameters of asphalt concrete. Moreover, the tests on the first group of four SCB samples made it possible to identify material parameters of the FE model. The estimated parameters were applied to verify the computational algorithm, comparing the numerical and laboratory results of the 32-specimen test group. The results confirmed the correct performance of the proposed model with respect to the test data. It is essential that the discussed model was focused on the breaking forces and fracture parameters, complemented by their scatter, as they are decisive in structural design.

2. Laboratory tests

To estimate fracture parameters of asphalt concrete, semi-circular test specimens (SCB) were subjected to three-point bending (Fig. 1). The test was based on the procedure included in the standard [8] and further modified on a literature basis [31]. Force F and vertical displacement d were measured throughout the tests (Fig. 1b). During testing, the specimen and the loading frame were located in a thermostatic chamber of the testing machine to achieve a constant test temperature of 10°C. The tests were performed on samples with one notch depth a = 10 mm, and the vertical displacement rate was 1 mm/min. Test conditions and specimen specifications were selected to capture the post-peak behavior accurately, which is essential for estimating fracture parameters.

a)

b)

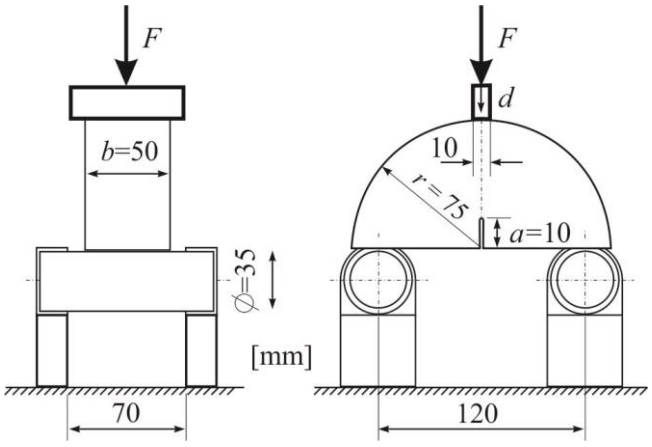

Fig. 1. Semi-circular SCB bending test (a) and its scheme (b)

2.1. Materials and test specimens

Road bitumen 50/70 [32] produced in a Polish refinery was selected for laboratory testing. This type of bitumen is widely used in Poland for wearing courses of roads with light and medium traffic (from 0.03×10^6 to 7.3×10^6 of 100 kN standard axle loads, which

correspond to 0.07×10^6 and 17.8×10^6 of 80 kN standard axle loads). Table 1 summarizes the properties of bitumen used in the research. Parameters are given for bitumen before aging (original) and after aging with the use of a rolling thin-film oven test (RTFOT) [33].

Table 1. Bitumen properties

Property		Result
Penetration at 25 °C 0.1 mm [34]	Original	54
	RTFOT	40
Softening point, Ring & Ball Temperature °C [35]	Original	50.8
	RTFOT	57.8
Performance Grade [36]		64–22
Fraass Breaking Point Temperature °C [37]	Original	−14
	RTFOT	−12

Laboratory tests were performed on asphalt concrete AC 11 S [38], designed for wearing course for medium traffic (from 0.5×10^6 to 7.3×10^6 of 100 kN standard axle loads). The mixture was designed according to the Polish technical guidelines [39]. The composition of the mixture is presented in Tables 2 and 3. Table 2 includes volumetric asphalt concrete distinction into a two-phase material model consisting of coarse aggregate and mortar (fine aggregate with filler, binder, and air voids), i.e., volume 52.8% and 47.2%, respectively. This additional distinction is decisive in FEM computations.

Table 2. Composition of asphalt concrete.

Property	Composition [%]			
	Mineral mix, by mass	Mineral-asphalt mix, by mass	Mineral-asphalt mix, by volume	FEM two-phase material mix, by volume
Coarse aggregate 8/11 (granite)	25.0	23.6	20.9	52.8
Coarse aggregate 5/8 (granite)	15.0	14.2	12.6	
Coarse aggregate 2/5 (granite)	23.0	21.7	19.3	
Fine aggregate 0/2 (granite)	30.0	28.3	25.1	47.2
Limestone filler (limestone)	7.0	6.6	5.9	
Bitumen 50/70	-	5.6	14.0	
Voids	-		2.2	

Table 3. Grading curve of asphalt concrete.

Grading curve	
Sieve size (mm)	% Passing (by mass)
16	100
11.2	98
8	77
5.6	62
4	52
2	39
0.125	11
0.063	7.2

Asphalt mixture was prepared using a laboratory mixer according to [40] and subjected to short-term aging before specimen compaction according to the procedure in Appendix 2 of [39] (three hours loose mix conditioning at 135°C before sample compaction). Samples for SCB testing were prepared using a gyratory compactor with a diameter of 150 mm and a height of 105 mm. The process was set to achieve 99% of Marshall sample density. Four SCB specimens were cut out from a single gyratory specimen. The cutting process is shown in Fig. 2. Information on sample geometry dispersion is presented in Table 4. These dimensions are within the tolerance range allowable by [8].

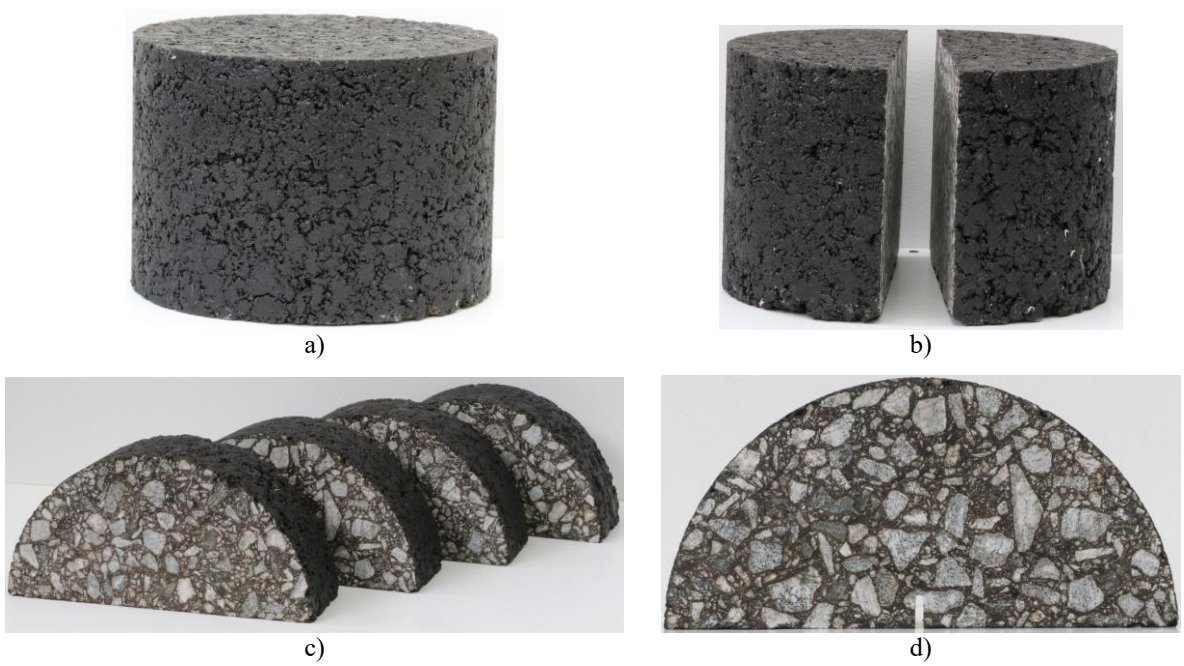

Fig. 2. Sample preparation process: a) gyratory compacted sample, b) two halves of one gyratory sample, c) four semi-circular specimens, d) final notched SCB sample

Table 4. Statistical data on the geometry of 4 (Series 1) and 32 (Series 2) specimens

Parameter	Final dimension, [mm]	Minimum value, [mm]	Maximum value, [mm]	Average, [mm]	Standard deviation, [mm]	Coefficient of variation, [-]
Series 1 – 4 specimens						
Height *r*	75	72.2	74.0	73.1	0.81	0.0110
Width 2*r*	150	148.0	148.2	148.1	0.12	0.0008
Depth *b*	50	50.9	51.3	51.1	0.21	0.0040
Notch *a*	10	7.5	9.8	8.5	1.2	0.1409
Series 2 – 32 specimens						
Height *r*	75	72.2	74.2	73.1	0.51	0.0069
Width 2*r*	150	147.3	149.1	148.4	0.50	0.0033
Depth *b*	50	49.7	42.4	51.0	0.76	0.0149
Notch *a*	10	8.0	9.7	8.8	0.48	0.0550

Both sample groups were prepared separately. It is essential to compare the results of test groups with the same composition but prepared during different production processes. The first test series consisted of four specimens only, which is a standard batch for such laboratory tests. The results of this test group were used as an identification basis for the FE model parameters. The second series of 32 specimens allowed for a precise statistical analysis of laboratory-based material parameters. Moreover, the 32-piece variant made it possible to verify the FE model based on the 4-piece experiment.

2.2. Test results

Figure 3 shows the *F–d* results, i.e., force *F* versus displacement *d*, in the initial series of four SCB laboratory tests. Adopted test parameters, i.e., loading rate (1 mm/min) and test temperature (+10°C), made it possible to record the entire *F–d* curve, including the softening zone (Fig. 3). In the case of other mixtures and parameters, e.g., negative temperatures, measurements, and loading rate should be controlled by the crack mouth opening displacement sensor (CMOD).

Based on the data shown in Fig. 3, the parameters that define the material toughness show substantial variability. Dispersion determined in the tests is represented by red curves denoting the mean values $\bar{F}$ and the triple standard deviations $F = \bar{F} \pm 3\sigma_F$ determined for every vertical displacement *d* (Fig. 3). The three-sigma rule means that almost all observed data (99.7%) falls within the range of three standard deviations of the mean. Note that in the limited specimen domain (four samples), the statistical information is qualitative only.

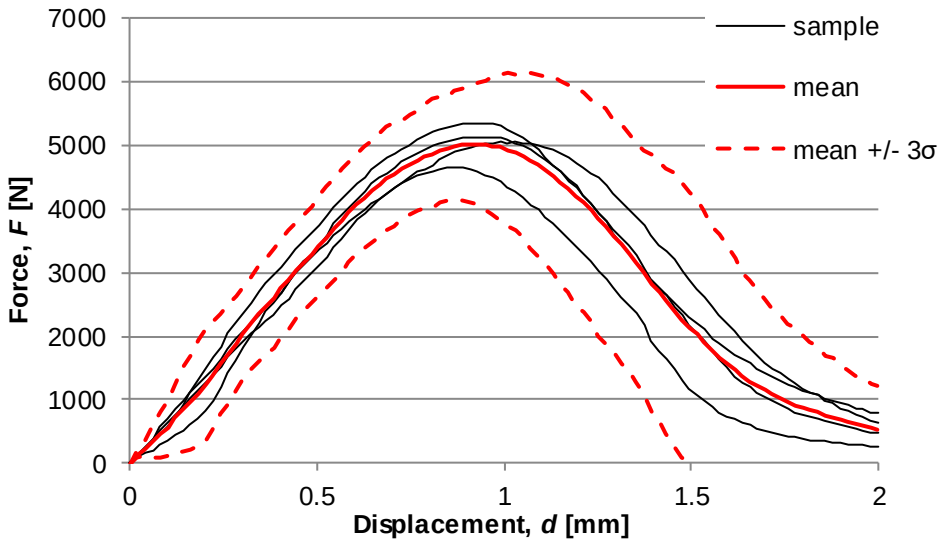

Fig. 3. Force-displacement *F–d* curves of four SCB specimens

Figure 4 shows the results of the second extended test group of 32 specimens. The diagrams are similar to the results of the first group of four samples (Fig. 3) in terms of initial stiffness scatter, maximum specimen loading, and softening curve. The shapes of curves presented in Fig. 4 justify using the three-sigma rule because every test result lies within the $F = \bar{F} \pm 3\sigma_F$ range.

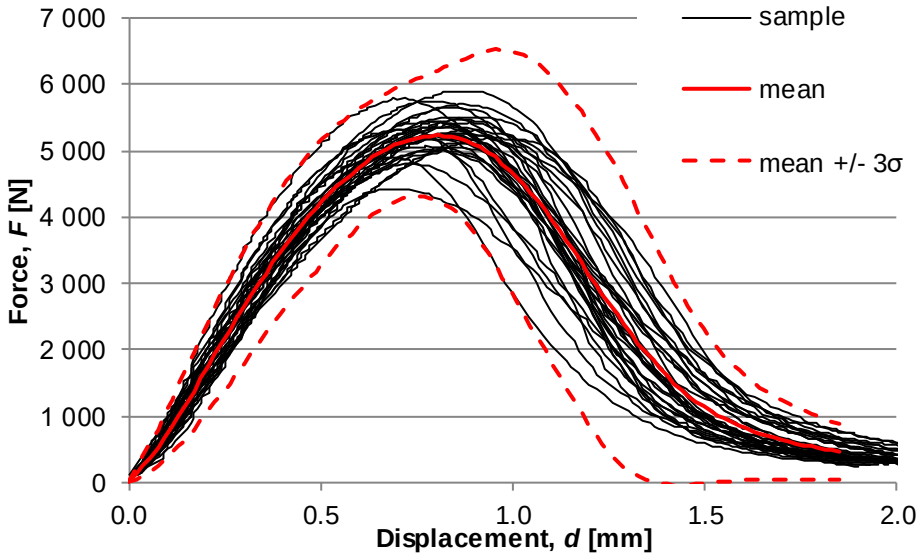

Fig. 4. Force-displacement *F–d* curves obtained for 32 tested SCB specimens

The major reason for fracture mechanics parameters dispersion of asphalt concrete is the random aggregate grading and its distribution within a specimen. Slight differences in specimen dimensions have an impact as well (Table 4). Examples of specimen damage

presented in Fig. 5 show various failure modes. The crack in most specimens is a distinct brittle fracture splitting that divides SCB specimen into two halves (Figs. 5a, b, and c). However, the specimen crack in Fig. 5d does not match this pattern, showing a quasi-plastic course. The cracks running through the aggregate (Fig. 5a) or the bitumen alone (Fig. 5c) are essential to note here. The identical damage course of SCB specimens is observed through the thickness of damaged samples. Thus the problem can be considered two-dimensional only, a treatment commonly used in numerical analysis.

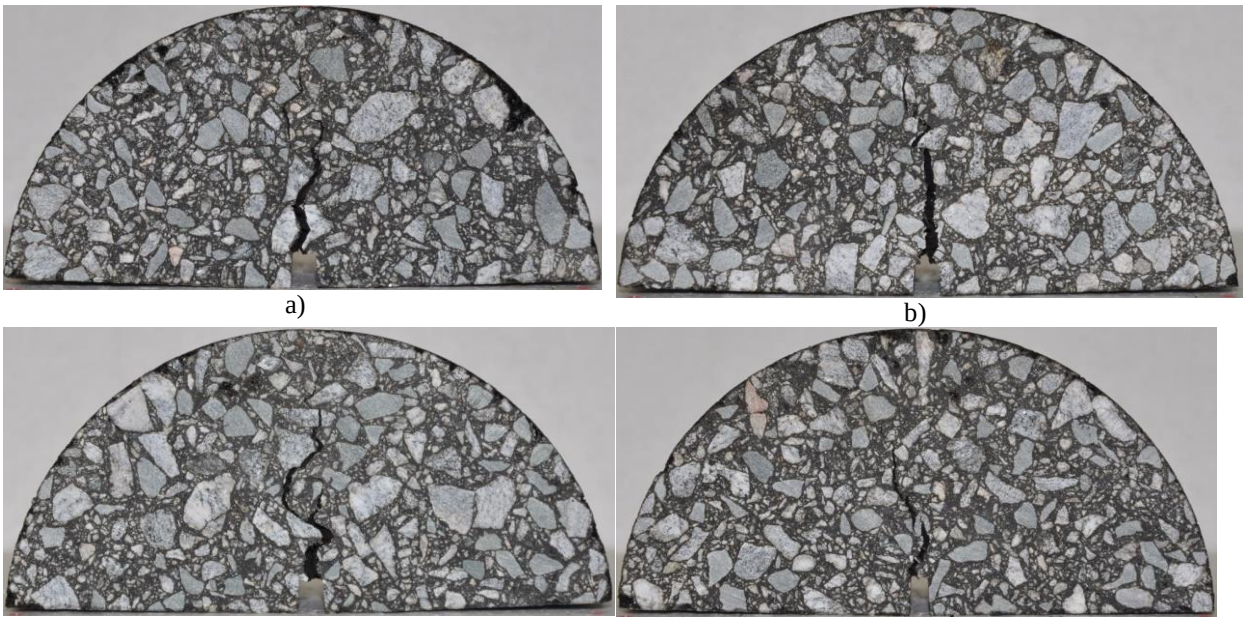

a) b) c) d)

Fig. 5. Examples of SCB specimens damaged in the test course (10 mm notch depth)

The laboratory tests make it possible to determine basic fracture toughness parameters of asphalt concrete. The critical stress intensity factor K_{IC} is calculated as follows

$$K_{IC} = \sigma_0 Y_I \sqrt{\pi a} \tag{1}$$

where: a - notch depth, σ_0 - extreme test stress, and Y_I - normalized stress intensity factor due to type I fracture (opening mode).

The extreme bending stress in the specimen σ_0 is calculated with the use of the following equation

$$\sigma_0 = \frac{F}{2rb} \tag{2}$$

where: F - maximum test force (peak load), r - specimen radius, and b - specimen thickness (Fig. 1).

The measured specimen dimensions and notch depth were incorporated in the σ_0 stress assessment (Table 4).

The normalized stress intensity factor Y_I was also computed with the use of equation

$$Y_I = 4.782 - 1.219\frac{a}{r} + 0.063\exp(7.045\frac{a}{r}) \quad (3)$$

Regarding dimensional dispersion of 32 specimens, the normalized stress intensity factor Y_I (Eq. 3) ranges from 4.781 to 4.785 (the mean value is 4.783).

Material performance during cracking development is precisely reflected by strain energy, indirectly computed with the help of force-displacement *F–d* curve, i.e., the integrated area under the curve. Two independent parameters were determined, i.e., pre-peak ($U_{pre\text{-}peak}$) and post-peak ($U_{post\text{-}peak}$) strain energy (Fig. 6). Subsequently, the total damage energy of the specimen is U_{total}. The pre-peak and post-peak slopes of the *F–d* chart were also estimated (Table 5 and 6). The pre-peak slope (S_1) represents the specimen stiffness, while the absolute value of the post-peak slope (S_2) is linked with crack propagation speed. The distinction of two phases, i.e., pre- and post-maximum loading, is aimed at accurately reflecting specimen mechanical performance and comparing it with the FEM results. The laboratory test results are collected in Tables 5 and 6; the list includes mean values, standard deviations, and coefficients of variation of all analyzed parameters.

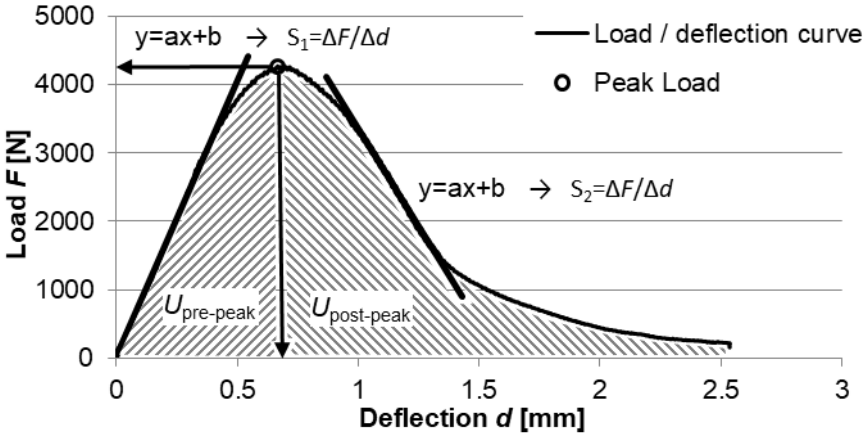

Fig. 6. Graphical interpretation of fracture mechanics parameters of SCB test

Table 5. Test results, initial series of 4 specimens

No.	F_{max} [N]	d [mm]	K_{IC} [N/mm$^{3/2}$]	$U_{pre\text{-}peak}$ [Nmm]	$U_{post\text{-}peak}$ [Nmm]	U_{total} [Nmm]	S_1 [N/mm]	S_2 [N/mm]
1	5359	0.92	16.4	2943	2990	5933	8465	7273
2	5133	0.92	17.9	2644	3317	5961	9000	6543
3	5056	1.18	15.6	3015	3126	6141	6081	6856
4	4651	0.85	16.0	2297	2423	4719	6676	6334
Mean value	5050	0.97	16.5	2725	2964	5689	7555	6751
Standard deviation	296	0.15	1.0	327	385	653	1398	409
Min value	4651	0.85	15.6	2297	2423	4719	6081	6334
Max value	5359	1.18	17.9	3015	3317	6141	9000	7273

Table 6. Test results, extended series of 32 specimens

No.	F_{max} [N]	d [mm]	K_{IC} [N/mm$^{3/2}$]	$U_{pre\text{-}peak}$ [Nmm]	$U_{post\text{-}peak}$ [Nmm]	U_{total} [Nmm]	S_1 [N/mm]	S_2 [N/mm]
1	5259	0.81	17.9	2647	3748	3748	10207	9249
2	5258	0.86	16.6	2805	2579	2579	9770	10099
3	4793	0.72	16.9	2015	2645	2645	9647	6937
4	5004	0.81	16.8	2502	2527	2527	8815	8503
5	5234	0.76	17.3	2377	2743	2743	9140	9009
6	5434	0.78	17.7	2334	3076	3076	9470	7054
7	4430	0.67	15.0	1713	2650	2650	8519	5604
8	5006	0.79	17.3	2422	2908	2908	9922	8051
9	5447	0.76	17.4	2492	2566	2566	10189	12590
10	5699	0.86	18.7	2946	3024	3024	8992	9828
11	4903	0.66	16.7	1961	2295	2295	10862	8649
12	5310	0.70	18.1	2288	2527	2527	10599	9374
13	5346	0.79	17.4	2659	2478	2478	9894	10912
14	5461	0.84	17.7	2821	2730	2730	9903	10748
15	5220	0.80	16.9	2494	2595	2595	8930	8936
16	5231	0.79	17.8	2478	2511	2511	9653	10420
17	5499	1.12	18.1	2796	2380	2380	8758	11173
18	5461	0.88	17.2	2853	3057	3057	8515	8765
19	5070	0.77	17.2	2375	2703	2703	9484	7785
20	5054	0.82	16.8	2532	2769	2769	8785	7484
21	5308	0.69	17.1	2208	2905	2905	12766	8023
22	5751	0.76	19.6	2481	2987	2987	11822	9975
23	5117	0.86	16.8	2555	2815	2815	7838	6363
24	5434	0.89	19.0	2856	3012	3012	8353	8312
25	5195	0.93	16.5	2936	2966	2966	8370	8507
26	5306	0.86	18.2	2734	3044	3044	8182	9640

27	5371	0.84	17.5	2717	2346	2346	10016	15427
28	5182	0.81	17.6	2658	2464	2464	9826	7612
29	5243	0.80	16.5	2378	2847	2847	9606	6746
30	5649	0.85	18.8	2806	2247	2247	9623	12836
31	5787	0.69	18.8	2410	3247	3247	13614	7716
32	5901	0.85	20.4	3000	3218	3218	11067	10107
Mean value	5293	0.81	17.6	2539	2769	2769	9723	9139
Standard deviation	299	0.09	1.0	298	323	323	1272	2035
Min value	4430	0.66	15.0	1713	2247	2247	7838	5604
Max value	5901	1.12	20.4	3000	3748	3748	13614	15427

Data in Table 6 and the *F–d* diagrams (Fig. 4) confirm notable variation of statistical parameters in a group of 32 samples, similar to that in the 4-sample case (Table 5, Fig. 3). For example, the estimated mean values and standard deviations of both series were 5293 N and 299 N (32 samples); in the second case, 5050 N and 296 N (four samples), the relative differences are 4.6% and 1.0%, respectively. The 32-samples results make it possible to conduct a comprehensive numerical analysis.

Laboratory results show notable fracture parameter dispersion, featuring the critical stress intensity factor K_{IC} and the fracture energy U_{total}. It may be stated that the random distribution of aggregate in the specimens has the most significant impact on the scatter of the results.

The scatter of obtained results may also be influenced by other factors, e.g., random sample dimensions (see Table 4). Considering this aspect, the notch depth *a* may be assumed as the most important, especially due to the scale effect. However, it is not decisive in the case of asphalt concrete samples with low heights. A more important factor is the location of the notch within discussed material. By analyzing cross-section areas of splitted samples, it can be said that a higher maximum load was obtained when the tip of the notch was at least partially located within grains of coarse aggregate, which induced cracking within the volume of the aggregate. If the tip of the notch was not found in such an area, the crack was starting to form within mortar volume, and the recorded maximum loads were significantly lower.

2.3. The mortar tension test

Advanced numerical analysis of asphalt concrete specimens makes it necessary to provide the software with material data of mixture components. An alternate solution is to use averaged effective moduli, i.e., to conduct material homogenization. However, this process should be based on measured data of component materials. The primary input data for the FE

analysis are Young's moduli and maximum tensile stresses. Due to dominant specimen fracture processes, the data concerning material compressive strength are not essential. Additional tests were conducted on mortar samples made of fine aggregate, filler, and bitumen in accordance with the asphalt concrete composition. These tests were conducted in a ductilometer according to [41] (Fig. 7) at the temperature of +10°C; the tensile displacement rate was 1 mm/min. This experiment was aimed to estimate material property values, so two specimens were tested only (Fig. 8).

a)

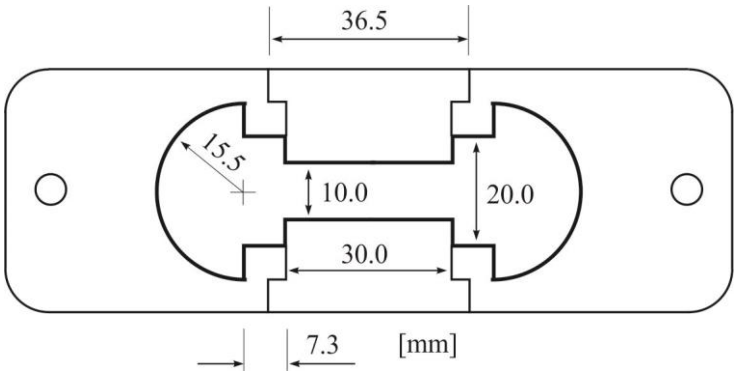

b)

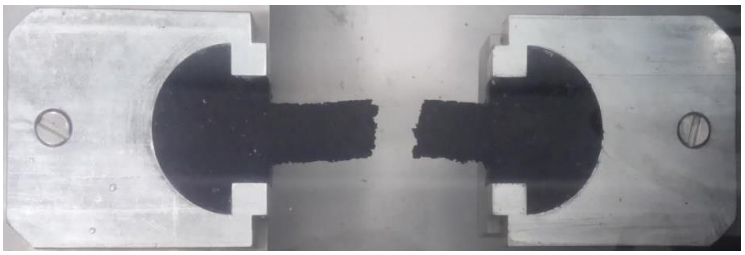

Fig. 7. Dimensions of a mortar specimen tested in a ductilometer (a) and a damaged specimen (b)

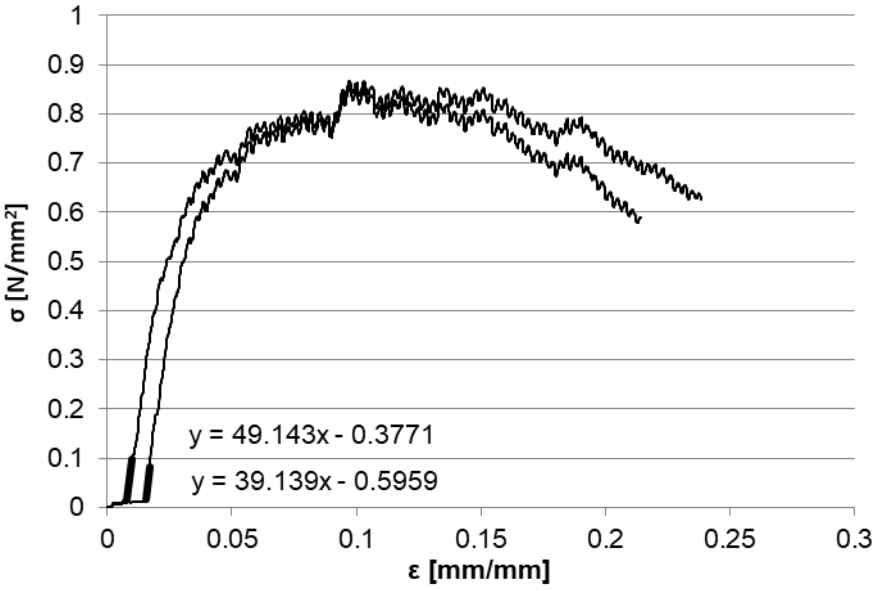

Fig. 8. σ–ε diagrams of the mortar tensile test

Both curves were linearised in the initial range (Fig. 8), and the value E_{mor} = 44 MPa was assumed as the mortar Young's modulus. Although the determined value is approximate only (precise strain measurements with the use of an extensometer were not conducted), it was assumed as initial data in the material property identification process for the FE procedure. It must be emphasized that the mechanical properties of asphalt mortar greatly depend on temperature and rate of deformation. If these parameters were to be changed, mortar Young's modulus would change and should be determined again.

3. The simulation-based FEM constitutive model

The main and most significant feature of the developed proprietary asphalt concrete material model is a simulation process that generates randomized input data for the FEM software. It was assumed that the FEM data generator should take into account not only the percentage content of individual mixture components but also the size of the aggregate. As a result, a random mixture structure is obtained, and thus the proposed algorithm can be described as a Monte Carlo material model. The proposed model would be used to determine global features of the asphalt mixture failure instead of the exact mapping of the cracking path. One of the first attempts of using a Monte Carlo material model was presented in [42].

An essential part of the model is adopting optimal sizes of finite elements. Following the laboratory specimen data (Tab. 2), a uniform aggregate and bitumen mortar was assumed, i.e., each contribution equals 50% instead of 52.8 and 47.2%. The two-phase model neglects air voids which contribute to the material volume only to a slight degree, thus not substantially affecting the global response of the loaded member. The adopted basic size of finite elements was 2×2 mm, which corresponds to the minimal size of coarse aggregate (see Table 2). Larger aggregate grains were obtained by joining finite elements of basic size into blocks. For the remaining elements, mortar properties were assigned.

The assumptions made during the construction of the FEM model were verified by performing intuitive mappings of the coarse aggregate distribution for a 40 × 40 mm portion of the SCB sample (Fig. 9a). This section refers to approximately 1/4 of the entire SCB specimen used in laboratory tests (150 × 75 × 50 mm). Afterward, a mesh with a size of 2 × 2 mm (Fig. 9b) was placed on the sample cross-section (Fig. 9b). A visual assessment was made as to whether the considered mesh element should be assigned with coarse aggregate or asphalt mortar characteristics. It was assumed that for an element to be classified as aggregate, its grains should cover at least 50% of the surface, not necessarily a single grain,

but the total share of aggregate grains in the area of 2 × 2 mm. The assumed FE model (Fig. 9c) can be considered a representative volume element (RVE).

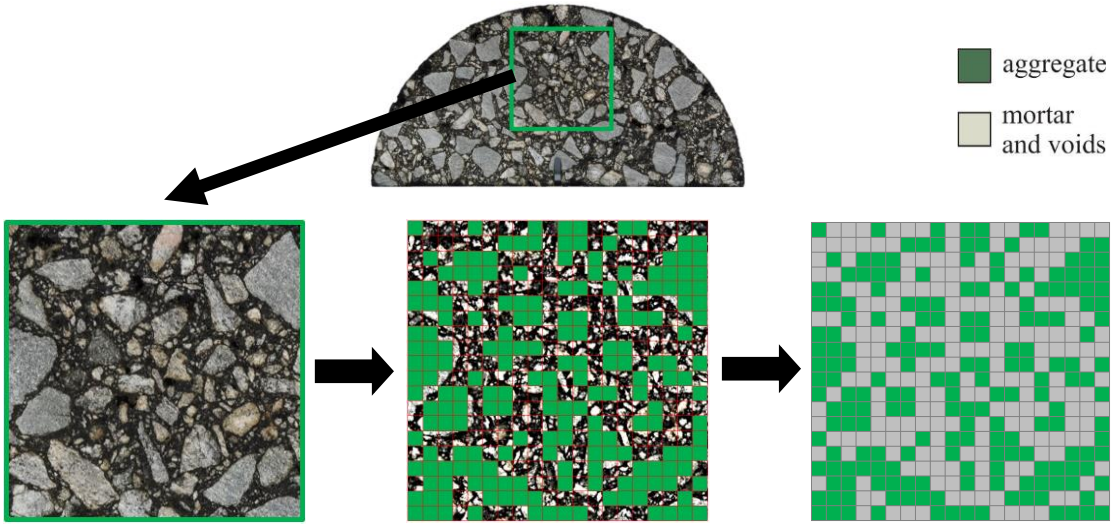

Fig. 9. Examples of material assignment based on the image of the actual sample; a) cut out fragment of the sample with dimensions of 40 × 40 mm, b) division into 2 × 2 mm elements with the selection of coarse aggregate, c) assignment of materials (coarse aggregate and asphalt mortar)

This type of identification process based on the analysis of the cross-section of actual samples can be fully automated by developing appropriate software. However, it does not seem practical because it could only be performed on a few prepared SCB specimens, which would not be correct from a statistical point of view. Therefore, adopting an appropriate simulation method without direct reference to identifying material distributions in the cross-sections of laboratory samples is justified.

The construction process of a FEM model with varying coarse aggregate and asphalt mortar structures consists of a random selection of elements. For this purpose, it is necessary to formulate an appropriate algorithm to prepare batch data for the FEM software. Two different methods of generating material parameter scatter were considered:

– simulation-based FEM model, i.e., direct random sampling of elements which are further linked with aggregate or bitumen parameters;

– random field model incorporating the generation of correlated fields, their transformed values make it possible to link the FE sample elements with aggregate parameters.

3.1 Simulation-based FEM model

Three different simulation-based FEM models were considered. The simplest model randomly assigns the material parameters of aggregate or bitumen mortar to finite elements (Fig. 10a). Uniformly distributed random numbers are generated and linked with aggregate and bitumen mortar material parameters. The result is a binarized image, frequent in sample analysis, e.g. [43]. Such an approach triggers a quasi-homogeneous material structure. In this case, no distinction is made between aggregate and bitumen mortar solids, i.e., merged groups of elements. The sampling procedure is conducted automatically in a distinct self-coded preprocessor for the ABAQUS data preparation [30].

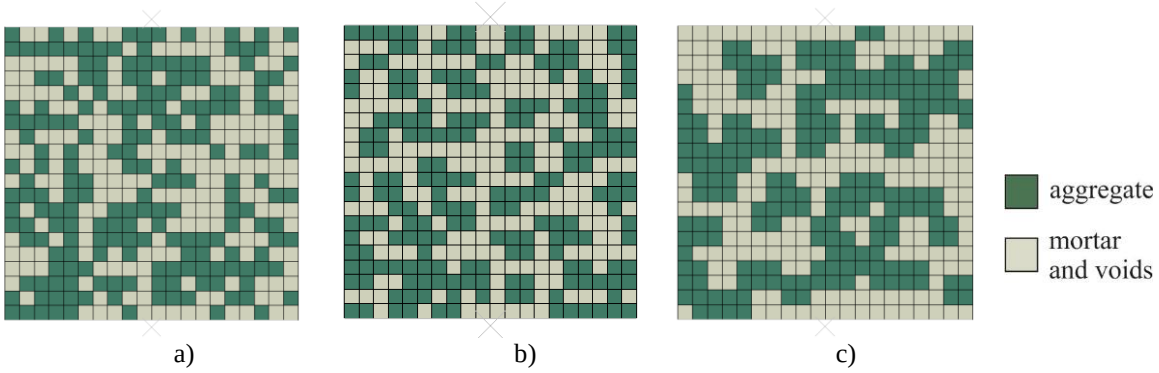

Fig. 10. Examples of asphalt concrete structure generation: a) uniformly distributed aggregate and mortar elements; b) joint element and node generation, the aggregate is assigned to all elements surrounding the generated node; c) elements surrounding the generated node are assigned the parameters of aggregate

The second generation mode regards the diversity of aggregate and bitumen mortar character (Fig. 10b). The algorithm conducts mixed node and element sampling of a FE model. Next, all elements meeting at a given node are assigned aggregate parameters, achieving 50% contribution of both materials in a sample. This is a way to simulate the aggregate solids of higher dimensions.

The third applied algorithm randomly generates the specimen nodes and assigns all neighboring elements with the aggregate material. This way, a merging effect is achieved, i.e., larger solids are formed (Fig. 10c). The number of elements randomly connected in a group may be considerably large. The generation process can match the material layout in the specimen, strictly correlated with the applied finite elements.

3.2 Generation of correlated fields

The second proposed method is more general; it incorporates the generation of correlated random fields. This approach makes it possible to shape the specimen structure by randomly merging the FE elements and linking them with the parameters of a chosen material, e.g., aggregate. The random field is defined by an exponential correlation function related to the first-order autoregression function or Markov process [44]

$$\rho(x, y) = \mathrm{e}^{-d_x|x|-d_y|y|} \tag{4}$$

where d_x and d_y are damping parameters capturing the correlation decay, $|x|$ and $|y|$ are the distances between field points along these axes.

Given d_x and d_y the correlation range between the model elements in the close vicinity of a point is adjusted to merge the elements in small or large groups with identical parameters. Other function types, e.g., the second-order non-homogeneous random field [44], simulates material stratification [45]. The random field generation was conducted by a self-created algorithm employing a conditional acceptance and rejection concept addressed in [46]. It should be noted that the FE model preparation makes it possible to employ any generation method and software, including commercial packages. Examples of the generated fields of various damping parameters are shown in Fig. 11.

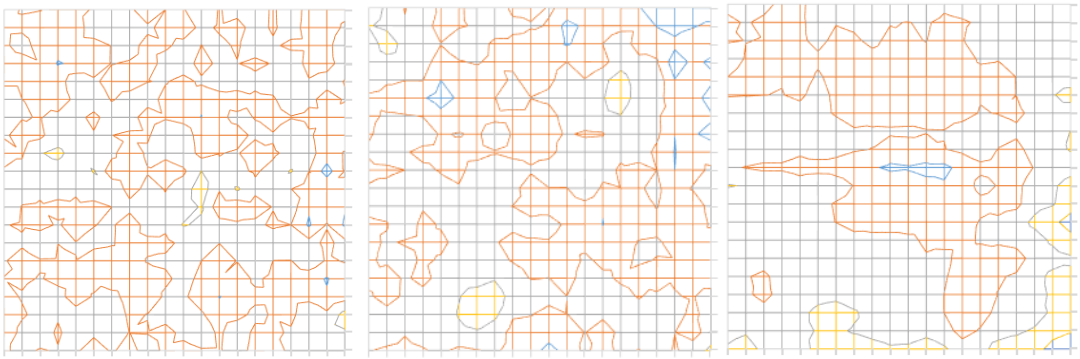

a) $d_x = d_y = 6\ \mathrm{m}^{-1}$ b) $d_x = d_y = 3\ \mathrm{m}^{-1}$ c) $d_x = d_y = 0.05\ \mathrm{m}^{-1}$

Fig. 11. Examples - generated fields of (a) weak, (b) medium, and (c) strong correlation

The generated field is relevantly transformed to conduct the asphalt concrete mixture simulation. The analyzed model distinguishes two materials in a section only; the generated material is divided according to the computed median, i.e., 50% of elements match every material. This process can be performed in two steps:

1) field values at discrete points (with coordinates in the centers of the elements) are arranged

in ascending order,

2) the median is determined, finite elements linked with the initial 50% values are defined with coarse aggregate parameters, the remaining ones represent asphalt mortar.

Generation in other proportions or with more materials may be conducted identically.

Assuming various correlation lengths (Fig. 11), highly diverse fields are obtained (Fig. 12). In the uncorrelated case (the so-called white noise), the field is identical with single element generation (Fig. 10a). Enhancing the generation domain means the formation of a large grain structure. In the case of $d_x = d_y = 6\ \mathrm{m}^{-1}$ the structure resembles the non-correlated case (Fig. 12a), while for $d_x = d_y = 3\ \mathrm{m}^{-1}$ (Fig. 12b) and $d_x = d_y = 0.05\ \mathrm{m}^{-1}$ (Fig. 12c), the elements are connected analytically.

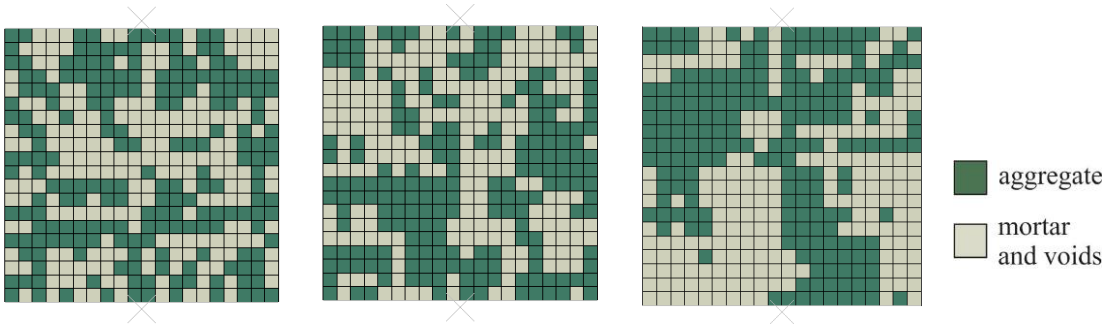

Fig. 12. Examples of asphalt concrete structure generation using random fields

The analysis of distribution examples yields that various mixture structures can be created by selecting the specific generation method. Note that the analyzed case distinguishes only two materials (aggregate and asphalt mortar), but in general, the number of material types is not limited. The final effect is a quasi-homogeneous structure (Fig. 10 and 12), not an actual mixture image (Fig. 5).

3.3 Randomly generated axially compressed sample

The outcome of the computational algorithm is illustrated by a uniaxial compression test simulation (Fig. 13). The specimen dimensions 40 × 40 mm and 2 mm finite element size (40 × 40 elements) were assumed in the computations. The load is subjected by a non-deformable body acting on the specimen without friction to allow unconstrained horizontal deformation (Fig. 13). The averaged material data for coarse granite aggregate, Young's moduli E_{agg} = 60000 MPa and Poisson's ratios ν_{agg} = 0.2, were assumed based on literature [47–49]. In the case of Young's modulus of mortar, the laboratory test results were incorporated (Chapter 2.3): E_{mor} = 44 MPa, ν_{mor} = 0.2. Plane stress was assumed in the computations.

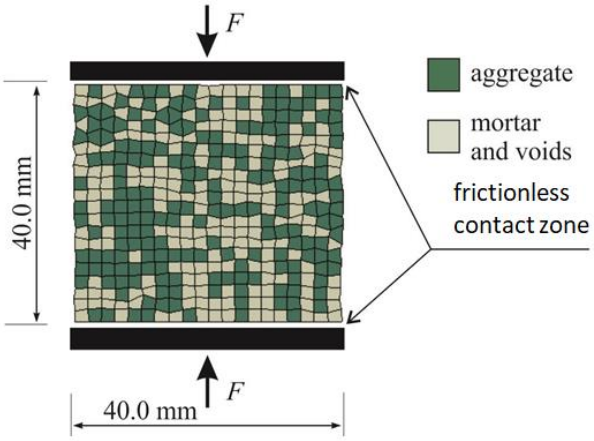

Fig. 13. Example of a randomly generated axially compressed sample

The computations assess the impact of uncertain material structure on the effective Young's modulus with regard to its scatter. Material parameters of aggregate or bitumen are randomly assigned to selected elements of the FE model. Generation routines described in Chapters 3.1 and 3.2 were applied. The ABAQUS results for FE models generated following Fig. 10 and Fig. 12 are listed in Table 7. The conducted analysis was preliminary; thus, only five computations were performed.

Table 7. Randomly generated axially compressed samples – comparison of results

	Simulation-based model			Random field model		
FEM model	Fig. 10a	Fig. 10b	Fig. 10c	Fig. 12a	Fig. 12b	Fig. 12c
Mean value $\bar{E}$ [MPa]	298.8	235.7	376.8	274.6	362.9	1769.3
Standard deviation σ_E [MPa]	45.7	54.0	208.0	27.7	118.3	2900.0

Based on provided numerical results, it can be concluded that both models – the simulation-based FEM model and the random field model – allow to freely adjust the effective Young's modulus mean value and standard deviation (Table 7). Moreover, appropriate parameter adjustment with the use of both models brings similar results. It is important to note that the random field model is more challenging to implement for engineering applications. Assigning a proper generation method and its parameters (e.g., damping parameters *d*) requires a dedicated preliminary analysis. For example, the numerical simulation results (Table 7) for the specimen generation shown in Fig. 12c are unrealistic. In this high correlation case, the generated aggregate may form jointed vertical structures resisting considerable compressive stresses.

The overall conclusion is that the proposed algorithm is capable of generating random data and causing result scatter. The range of random response may be adjusted by FE model

modification too. Model and parameter identification is conducted by a trial and error routine, using laboratory results. Therefore the proposed FE material model may be described as a Monte Carlo simulation-based constitutive model. Similar solutions can also be used in three-dimensional soil modeling [50].

4. Material parameter identification of SCB specimens

The laboratory test results (Fig. 3 and 4) lead to quasi elastic-brittle material constitutive relations. The non-linear solution results from diverse material parameters linked with finite elements and the cohesive joint used to simulate the crack propagation. Hence the implemented model is phenomenological in its nature. The FE model of the SCB specimen (plane stress) is shown in Fig. 14.

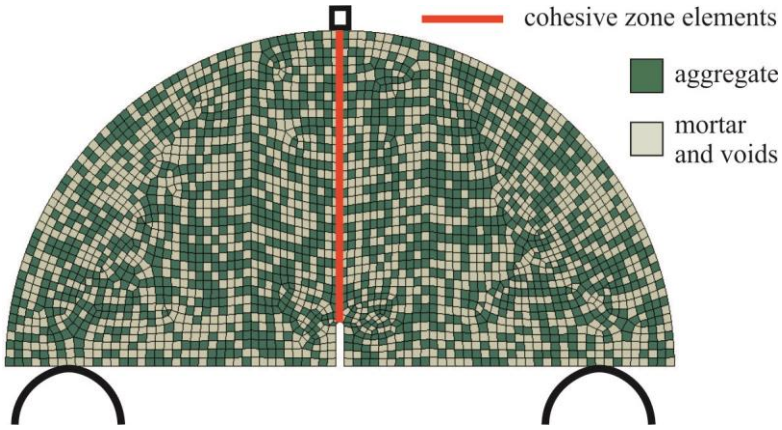

Fig. 14. FEM model of SCB notch specimen (ABAQUS)

The element dimensions are close to 2 mm, corresponding to the lowest coarse aggregate dimension (Tab. 3). The quasi-uniform element layout was provided in the specimen domain (Fig. 14). The FE mesh was not densified at the vicinity of the notch vertex and the crack propagation zone because the fracture development is traced by cohesive elements joining two specimen halves (Fig. 14). Note that the analysis is not aimed at reflecting the damage mechanism of any given specimen precisely; it only assesses global characteristics of damage. A simulation-based fictitious constitutive model was applied to simulate the material (Fig. 10a), i.e., individual elements were sampled and assigned with Young's modulus of aggregate or bitumen in 50/50% grading (Tab. 2). Thus it was the simplest random model to assess the capability of reflecting actual laboratory results. The discussed model does not take into account the random nature of the dimensions of the samples and depth of the notch because these parameters have a much smaller impact on the results of the analysis compared to the distribution of aggregate in the SCB sample.

The cohesive fracture contact model (Fig. 15) was applied at the specimen symmetry axis (Fig. 14). In natural conditions (Fig. 5), crack propagation along the notch line (notch extension) is not dominant because of aggregate layout; however, it is one of the possible scenarios (Fig. 5b). In search of global material characteristics, such an approximate approach is sufficient and frequent in numerical analysis. The parameters of the cohesive joint are assumed constant (i.e., deterministic); hence the model is simplified. Shear stiffness and failure stress components were assumed high enough to exclude shear failure.

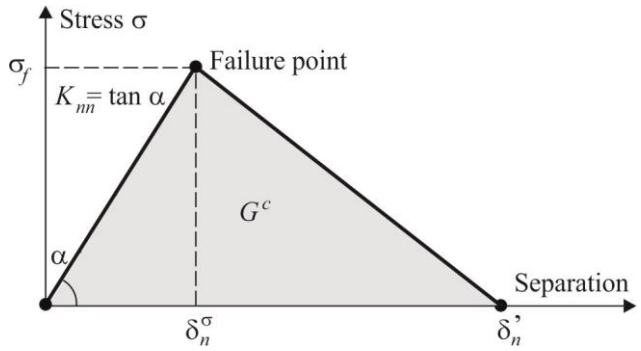

Fig. 15. Cohesive contact linear damage evolution model [30]

Since the entire data set for both aggregate and bitumen is not available, a series of numerical tests were conducted to adjust the FEM results to experimental relations. Material parameter identification of SCB specimens was conducted based on 4-item experimental results (Fig. 3). Since the result domain is small, additional curves were determined to represent an average of the *F–d* diagrams and their triple standard deviations (Fig. 3). The identification process of model parameters is considered complete if the numerical results are located in the prescribed region. It is not possible here to apply other criteria involving error minimization. The approximation process of numerical results for laboratory testing concerns selected parameters (elastic performance, extreme force, fracture, and softening) in probabilistic terms, so their mean values and standard deviations are sought. Part of the data is conjugate while the remaining part is not; this qualitative diversity makes the identification process problematic.

Material parameter generation for individual elements was conducted in the self-made pre-processor by modifying the ABAQUS software input files [30]. The first approximation started with the following literature-based material data: for aggregate E_{agg} = 60000 MPa and obtained from laboratory tests of mortar E_{mor} = 44 MPa, $\nu_{agg} = \nu_{mor}$ = 0.2 (Chapter 3). Next, in the course of a trial and error identification process (several iterations involved), the parameters of Young's moduli (E_{agg}, E_{mor}) were altered to model the initial (linear) system

stiffness and cohesive parameters to reflect the maximum force of the test and material softening (Fig. 3). The results obtained for a group of four numerical samples are presented in Fig. 16. The following material data were estimated in the process: E_{agg} = 60000 MPa, E_{mor} = 160 MPa, $\nu_{agg} = \nu_{mor} = 0.2$, $K_{nn} = 10^{10}$, σ_f = 2.3 MPa, G^c = 0.0022 J (Fig. 15) with a damage stabilization parameter (viscosity coefficient) η = 1e-04. Both the aggregate and the asphalt mortar were described with a linear elastic model. In the case of asphalt mortar, its properties depend on external conditions. Therefore, this approach is possible only with the analysis limited to a constant temperature and load speed. It should be emphasized that the laboratory tests were performed in such conditions (+ 10 ° C, 1 mm/min).

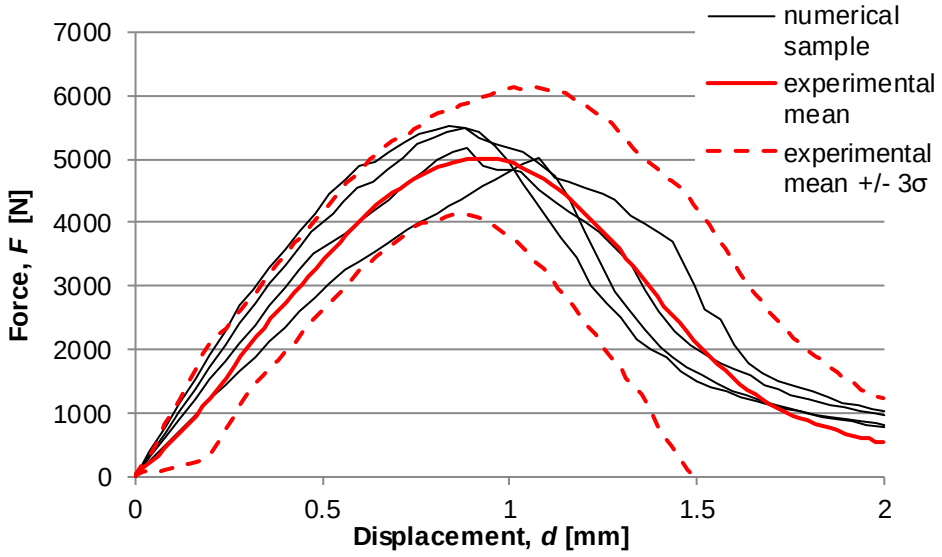

Fig. 16. Experimental results vs. FE computation 4-item variant results

The shapes of diagrams in Fig. 16 allow to consider the identification process satisfactory, but the laboratory results are only partially reflected. Note that the entirety of laboratory-based and numerical results are random. Statistical inference based on four samples is not reliable; thus, the identification process is approximate here. Variation of mortar Young's modulus E_{mor} = 160 MPa with regard to tensile test results E_{mor} = 44 MPa (Chapter 3) is substantial. It is justified by the low precision of the tensile tests without an extensometer. Young's modulus was assessed by the stress-strain diagram only (Fig. 8). Moreover, it is problematic to derive a relation between the bitumen and aggregate Young's moduli and the global stiffness of the analyzed SCB specimen. It comes from the difference between the static systems of the models, i.e., bending assumed instead of tension. Due to SCB specimen dimensions (the depth-width ratio), the stress distribution resembles more complex plane

stress instead of a beam model. Other parameters show their values close to the experimental and literature data.

The selection and calibration process of the FE material model was concluded at this stage. Complementary laboratory tests involving 32 pieces (Fig. 4) were further employed to verify the FE model.

5. Fracture toughness parameter estimation supported by FEM models

The estimated material parameters of the FEM model were directly introduced into the analysis of 32 SCB specimens (Fig. 4). The computations aim at a possibility to reflect basic asphalt concrete parameters with their scatter by a model based on limited laboratory data (four pieces only). Note that the laboratory results of four specimens serving as a base for the FEM parameter estimation (Fig. 3, Table 5) differ slightly from those based on 32 samples (Fig. 4, Table 6) investigated at a different time, though in accordance with the same recipe and conditions. Such an approach reflects the actual preparation process of asphalt concrete mixture because the material is usually prepared in various periods. Therefore, both the proposed identification procedure of material parameters and computer simulations refer to actual manufacturing conditions of asphalt concrete. The algorithm of conducted laboratory tests and a two-stage FE analysis is presented in Fig. 17.

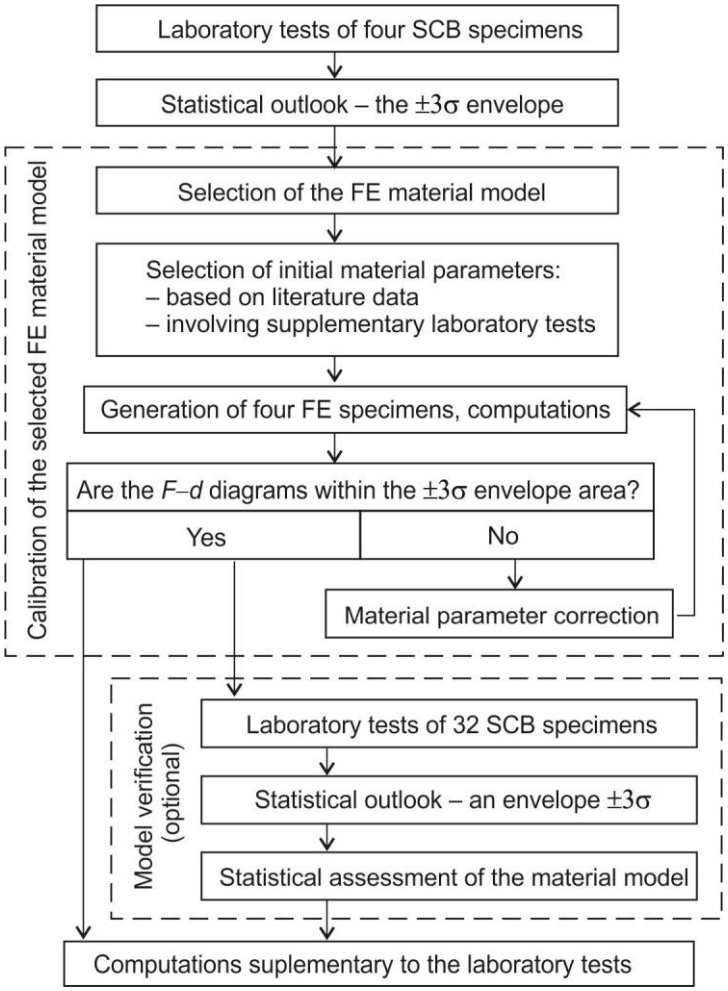

Fig. 17. Calibration and verification scheme of the FE material model

The computations were conducted on a 32-item batch; their results were compared with the laboratory outcomes (Fig. 18, Table 8). Similarly to the laboratory tests, such a limited realization domain is insufficient for a satisfactory Monte Carlo convergence. While it is easy to expand the realization domain, a larger number of laboratory specimens takes extra expenditure; thus, it is unjustified. Numerical computations are aimed to map laboratory tests using the same number of samples.

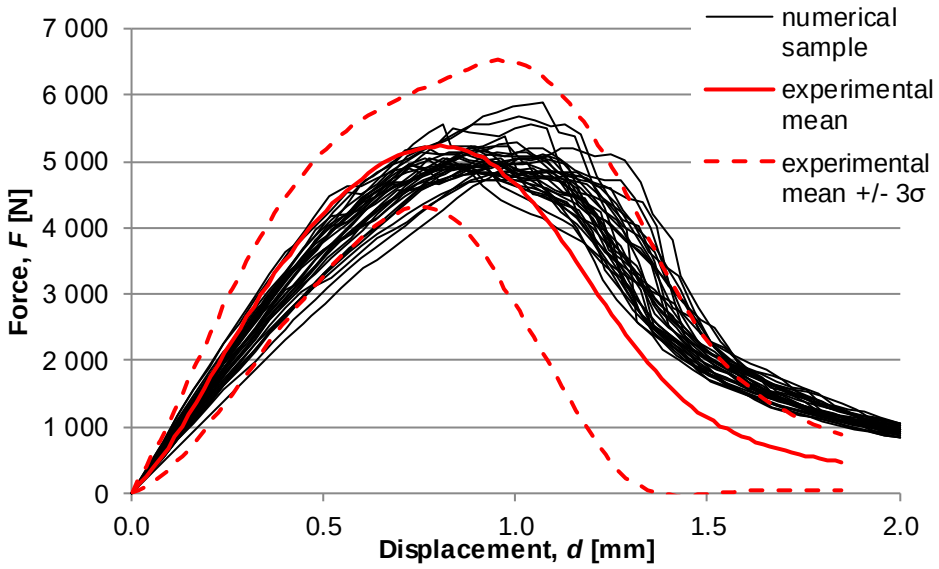

Fig. 18. FEM results (32 samples) and the triple standard deviations

Table 8. Laboratory test results vs. numerical simulations (32 specimens group)

Parameter	Statistical description	Laboratory tests	Numerical simulations	Error [%]
F_{max} [N]	Mean value	5293	5159	2.5
	Standard deviation	299.3	263.5	11.9
	COV	0.057	0.051	
d [mm]	Mean value	0.81	0.93	15.3
	Standard deviation	0.088	0.116	32.0
	COV	0.109	0.125	
K_{IC} [N/mm$^{3/2}$]	Mean value	17.6	18.4	4.9
	Standard deviation	1.05	0.94	10.0
	COV	0.059	0.051	
$U_{pre\text{-}peak}$ [Nmm]	Mean value	2539	2 924	15.2
	Standard deviation	298.4	507.3	70.0
	COV	0.118	0.173	
$U_{post\text{-}peak}$ [Nmm]	Mean value	2769	2 902	4.8
	Standard deviation	322.9	475.0	47.1
	COV	0.117	0.164	
U_{total} [Nmm]	Mean value	5308	5 826	9.8
	Standard deviation	482.7	139.8	71.0
	COV	0.091	0.024	
S_1 [N/mm]	Mean value	9723	7 662	21.2
	Standard deviation	1272.1	831.0	34.7
	COV	0.131	0.108	
S_2 [N/mm]	Mean value	9 139	8 766	4.1
	Standard deviation	2035.0	2 550.0	25.3
	COV	0.223	0.291	

The laboratory and FEM results (Fig. 18, Tab. 8) cannot be compared explicitly. Selected parameters, e.g., maximum force F or critical stress intensity factor K_{IC} are sufficiently represented by their mean values; however, their standard deviations are dispersed. Other basic parameters, e.g., mean deflection d corresponding to the maximum force F, is linked with a relatively high error. A crude outlook at the simulation-based graphs (Fig. 16) shows that the numerical results reflect the experimental scatter only partially. The numerical solutions are shifted with regard to the laboratory result envelope (Fig. 18). This is because the material parameters were calibrated by the four-sample laboratory test. Since the 32 experimental samples were produced as a separate batch, the simulation results can be considered satisfactory. The computations produce individual *F-d* diagrams, but the primary aim of the analysis is to estimate the mean value and standard deviation of fracture mechanics parameters. These values are decisive in the design of concrete asphalt mixtures and pavements. The results based on the presented model are bound to expand the laboratory-based information on the anticipated dispersion of asphalt mixture material parameters.

6. Conclusions

This work presents the study of fracture mechanics parameters of asphalt concrete measured in the laboratory tests and estimated during computational analysis. The proposed two-phase model is based on a random distribution of material parameters and takes into account the scatter of laboratory test results. The conducted laboratory and numerical experiments allow to draw the following conclusions:

1. Two experimental series conducted on four and 32 asphalt concrete SCB specimens detect a substantial result dispersion with regard to extreme breaking load, elastic parameters, fracture toughness, and the softening curve. The estimated standard deviations are high enough to consider them obligatory in the design process.
2. The laboratory tests can be readily supported by numerical simulations, and a computational algorithm is formed to reflect the SCB laboratory tests with regard to the result scatter. The authors' FE model is introduced, simplifying the specimen generation (mortar and aggregate parameters) by Monte Carlo simulation.
3. Standard laboratory tests of four SCB specimens, enhanced by the literature data, make it possible to define basic FEM model parameters.
4. The proposed two-phase FEM material model is not intended to precisely reflect the damage process of a single laboratory specimen. It is aimed at achieving global material

characteristics and their scatter. Upon this assumption, the model may be applied for large structures, e.g., parts of road pavements critical for fatigue life and general performance.

5. The presented computational algorithms may be applied in the design process of pavements overlay.
6. The presented simulation-based fictitious constitutive model may be incorporated in the analysis of heterogeneous materials such as concrete and rocks.

Acknowledgments

The authors acknowledge the access to computational software provided by the Centre of Informatics – Tricity Academic Supercomputer & networK (CI TASK) and the financial support by the Innovative Economy Operational Programme [POIG.01.04.00-24-073/09-03].

References

[1] G. Nsengiyumva, T. You, Y.-R. Kim, Experimental-Statistical Investigation of Testing Variables of a Semicircular Bending (SCB) Fracture Test Repeatability for Bituminous Mixtures, J. Test. Eval. 45 (2017) 20160103. doi:10.1520/JTE20160103.

[2] N. Bala, M. Napiah, Fatigue life and rutting performance modelling of nanosilica/polymer composite modified asphalt mixtures using Weibull distribution, Int. J. Pavement Eng. 21 (2020) 497–506. doi:10.1080/10298436.2018.1492132.

[3] P. Singh, A.K. Swamy, Probabilistic approach to characterise laboratory rutting behaviour of asphalt concrete mixtures, Int. J. Pavement Eng. 21 (2020) 384–396. doi:10.1080/10298436.2018.1480780.

[4] P.J. Haghighat Pour, M.R.M. Aliha, M.R. Keymanesh, Evaluating mode I fracture resistance in asphalt mixtures using edge notched disc bend ENDB specimen with different geometrical and environmental conditions, Eng. Fract. Mech. 190 (2018) 245–258. doi:10.1016/j.engfracmech.2017.11.007.

[5] D.X. Lu, H.H. Bui, M. Saleh, Effects of specimen size and loading conditions on the fracture behaviour of asphalt concretes in the SCB test, Eng. Fract. Mech. 242 (2021) 107452. doi:10.1016/j.engfracmech.2020.107452.

[6] S. Pirmohammad, M. Abdi, M.R. Ayatollahi, Mode II fracture tests on asphalt concrete at different temperatures using semi-circular bend specimen loaded by various types of supports, Theor. Appl. Fract. Mech. 116 (2021) 103089. doi:10.1016/j.tafmec.2021.103089.

[7] AASHTO TP105-13, Standard Method of Test for Determining the Fracture Energy of Asphalt Mixtures Using the Semicircular Bend Geometry (SCB), Am. Assoc. State Highw. Transp. Off. (2013).

[8] EN 12697-44, Bituminous mixtures. Test methods for hot mix asphalt. Crack propagation by semi-circular bending test., (2010).

[9] R. West, C. Rodezno, F. Leiva, F. Yin, Development of a Framework for Balanced Mix Design, Final report to the NATIONAL COOPERATIVE HIGHWAY RESEARCH PROGRAM (NCHRP), Project NCHRP 20-07/Task 406, National Center for Asphalt Technology at Auburn University, Auburn, AL, 2018.

[10] B. Doll, H. Ozer, J. Rivera-Perez, I.L. Al-Qadi, J. Lambros, Damage zone development in heterogeneous asphalt concrete, Eng. Fract. Mech. 182 (2017) 356–371. doi:10.1016/j.engfracmech.2017.06.002.

[11] R. Ktari, A. Millien, F. Fouchal, I.-O. Pop, C. Petit, Pavement interface damage behavior in tension monotonic loading, Constr. Build. Mater. 106 (2016) 430–442. doi:10.1016/j.conbuildmat.2015.12.020.

[12] Y. Huang, D. Yan, Z. Yang, G. Liu, 2D and 3D homogenization and fracture analysis of concrete based on in-situ X-ray Computed Tomography images and Monte Carlo simulations, Eng. Fract. Mech. 163 (2016) 37–54. doi:10.1016/j.engfracmech.2016.06.018.

[13] P. Liu, J. Hu, D. Wang, M. Oeser, S. Alber, W. Ressel, G. Canon Falla, Modelling and evaluation of aggregate morphology on asphalt compression behavior, Constr. Build. Mater. 133 (2017) 196–208. doi:10.1016/j.conbuildmat.2016.12.041.

[14] M.R.M. Aliha, H. Ziari, B. Mojaradi, M.J. Sarbijan, Modes I and II stress intensity factors of semi-circular bend specimen computed for two-phase aggregate/mastic asphalt mixtures, Theor. Appl. Fract.

Mech. 106 (2020) 102437. doi:10.1016/j.tafmec.2019.102437.
[15] J. Wimmer, B. Stier, J.-W. Simon, S. Reese, Computational homogenisation from a 3D finite element model of asphalt concrete—linear elastic computations, Finite Elem. Anal. Des. 110 (2016) 43–57. doi:10.1016/j.finel.2015.10.005.
[16] T. Schüler, R. Jänicke, H. Steeb, Nonlinear modeling and computational homogenization of asphalt concrete on the basis of XRCT scans, Constr. Build. Mater. 109 (2016) 96–108. doi:10.1016/j.conbuildmat.2016.02.012.
[17] X.S. Shi, I. Herle, Modeling the compression behavior of remolded clay mixtures, Comput. Geotech. 80 (2016) 215–225. doi:10.1016/j.compgeo.2016.07.007.
[18] T. Kanit, S. Forest, I. Galliet, V. Mounoury, D. Jeulin, Determination of the size of the representative volume element for random composites: statistical and numerical approach, Int. J. Solids Struct. 40 (2003) 3647–3679. doi:10.1016/S0020-7683(03)00143-4.
[19] D.V. Griffiths, J. Paiboon, J. Huang, G.A. Fenton, Homogenization of geomaterials containing voids by random fields and finite elements, Int. J. Solids Struct. 49 (2012) 2006–2014. doi:10.1016/j.ijsolstr.2012.04.006.
[20] X.F. Wang, Z.J. Yang, J.R. Yates, A.P. Jivkov, C. Zhang, Monte Carlo simulations of mesoscale fracture modelling of concrete with random aggregates and pores, Constr. Build. Mater. 75 (2015) 35–45. doi:10.1016/j.conbuildmat.2014.09.069.
[21] D. Castillo, S. Caro, M. Darabi, E. Masad, Studying the effect of microstructural properties on the mechanical degradation of asphalt mixtures, Constr. Build. Mater. 93 (2015) 70–83. doi:10.1016/j.conbuildmat.2015.05.108.
[22] H. Li, Z. Yang, B. Li, J. Wu, A phase-field regularized cohesive zone model for quasi-brittle materials with spatially varying fracture properties, Eng. Fract. Mech. 256 (2021) 107977. doi:10.1016/j.engfracmech.2021.107977.
[23] P. Pan, F. Su, H. Chen, S. Yan, X. Feng, F. Yan, Uncertainty analysis of rock failure behaviour using an integration of the probabilistic collocation method and elasto-plastic cellular automaton, Acta Mech. Solida Sin. 28 (2015) 536–555. doi:10.1016/S0894-9166(15)30048-3.
[24] J. Ren, L. Sun, Characterizing air void effect on fracture of asphalt concrete at low-temperature using discrete element method, Eng. Fract. Mech. 170 (2017) 23–43. doi:10.1016/j.engfracmech.2016.11.030.
[25] M.A. Elseifi, L.N. Mohammad, H. Ying, S. Cooper, Modeling and evaluation of the cracking resistance of asphalt mixtures using the semi-circular bending test at intermediate temperatures, Road Mater. Pavement Des. 13 (2012) 124–139. doi:10.1080/14680629.2012.657035.
[26] E. Mahmoud, S. Saadeh, H. Hakimelahi, J. Harvey, Extended finite-element modelling of asphalt mixtures fracture properties using the semi-circular bending test, Road Mater. Pavement Des. 15 (2014) 153–166. doi:10.1080/14680629.2013.863737.
[27] S.M. Motevalizadeh, H. Rooholamini, Cohesive zone modeling of EAF slag-included asphalt mixtures in fracture modes I and II, Theor. Appl. Fract. Mech. 112 (2021) 102918. doi:10.1016/j.tafmec.2021.102918.
[28] H. Wang, J. Wang, J. Chen, Micromechanical analysis of asphalt mixture fracture with adhesive and cohesive failure, Eng. Fract. Mech. 132 (2014) 104–119. doi:10.1016/j.engfracmech.2014.10.029.
[29] J. Kollmann, G. Lu, P. Liu, Q. Xing, D. Wang, M. Oeser, S. Leischner, Parameter optimisation of a 2D finite element model to investigate the microstructural fracture behaviour of asphalt mixtures, Theor. Appl. Fract. Mech. 103 (2019) 102319. doi:10.1016/j.tafmec.2019.102319.
[30] M. Smith, ABAQUS/Standard User's Manual, Version 6.9, Dassault Systèmes Simulia Corp, Providence, RI, 2009.
[31] M. Pszczoła, C. Szydłowski, Influence of Bitumen Type and Asphalt Mixture Composition on Low-Temperature Strength Properties According to Various Test Methods, Materials 11 (2018).
[32] EN 12591, Bitumen and bituminous binders. Specifications for paving grade bitumens., (2010).
[33] EN 12607-1, Bitumen and bituminous binders. Determination of the resistance to hardening under influence of heat and air. Part 1: RTFOT method., (2014).
[34] EN 1426, Bitumen and bituminous binders. Determination of needle penetration., (2015).
[35] EN 1427, Bitumen and bituminous binders. Determination of the softening point. Ring and Ball method., (2015).
[36] AASHTO M 320, Standard Specification for Performance-Graded Asphalt Binder., Am. Assoc. State Highw. Transp. Off. (2021).
[37] EN 12593, Bitumen and bituminous binders. Determination of the Fraass breaking point., (2015).
[38] EN 13108-1, Bituminous mixtures. Material specifications Asphalt Concrete., (2016).
[39] WT-2 2014, Technical Guidelines, Asphalt Pavements on State Roads, Asphalt Mixes., Gen. Dir. Natl. Roads Mot. (2014).
[40] EN 12697-35, Bituminous mixtures. Test methods Laboratory mixing., (2016).

[41] EN 13589, Bitumen and bituminous binders. Determination of the tensile properties of modified bitumen by the force ductility method., (2018).
[42] C. Szydłowski, J. Górski, M. Stienss, Ł. Smakosz, The statistical impact of experimental result scatter of asphalt mixtures on their numerical modelling, MATEC Web Conf. 262 (2019) 05014. doi:10.1051/matecconf/201926205014.
[43] A. Bozorgzad, H. "David" Lee, Consistent distribution of air voids and asphalt and random orientation of aggregates by flipping specimens during gyratory compaction process, Constr. Build. Mater. 132 (2017) 376–382. doi:10.1016/j.conbuildmat.2016.10.112.
[44] W. Knabe, J. Przewłócki, G. Różyński, Spatial averages for linear elements for two-parameter random field, Probabilistic Eng. Mech. 13 (1998) 147–167. doi:10.1016/S0266-8920(97)00015-5.
[45] D. Castillo, S. Caro, Probabilistic modeling of air void variability of asphalt mixtures in flexible pavements, Constr. Build. Mater. 61 (2014) 138–146. doi:10.1016/j.conbuildmat.2014.02.075.
[46] E. Bielewicz, J. Górski, Shells with random geometric imperfections simulation — based approach, Int. J. Non. Linear. Mech. 37 (2002) 777–784. doi:10.1016/S0020-7462(01)00098-1.
[47] R.N. Schock, A.E. Abey, H.C. Heard, H. Louis, Mechanical properties of granite from the Taourirt Tan Afella Massif, Algeria., Livermore, California, 1972. doi:10.2172/4587622.
[48] C. Ljunggren, O. Stephansson, O. Alm, H. Hakami, U. Mattila, Mechanical properties of granitic rocks from Gidea Sweden, Technical report 85-06. University of Lulea, Sweden., 1985.
[49] M.C. Villeneuve, M.J. Heap, A.R.L. Kushnir, T. Qin, P. Baud, G. Zhou, T. Xu, Estimating in situ rock mass strength and elastic modulus of granite from the Soultz-sous-Forêts geothermal reservoir (France), Geotherm. Energy. 6 (2018) 11. doi:10.1186/s40517-018-0096-1.
[50] K. Żyliński, K. Winkelmann, J. Górski, The Effect of the Selection of Three-Dimensional Random Numerical Soil Models on Strip Foundation Settlements, Appl. Sci. 11 (2021) 7293. doi:10.3390/app11167293.